Tr. J. of Engineering and Environmental Science
23 (1999) , 317 – 337.
© TÜBİTAK

Elastic-Plastic Analysis of the Compression Bond of Column Bars in Foundations

Mahmut TURAN
D.P.Ü. Mühendislik Fakültesi, İnşaat Bölümü,
Yapı Anabilim Dalı, Kütahya-TURKEY

Received 01.05.1997

Abstract

An elastic-plastic analysis of the compression bond of column longitudinal reinforcement in bases is presented. In this analysis, slip failure of the ribbed reinforcing bars due to shear stresses between bar and concrete is considered. On the basis of the Mindlin equation, in conjunction with finite difference calculus, expressions are derived for the distribution of bond stress, load-vertical displacement relationship of the column bars in the anchorage length, and the failure load of the foundation. The theoretical solutions are in good agreement with the experimental results and the distribution of bond stress is shown to be significantly influenced by the bar stiffness factor, K.

Key Words: Foundation, deformed reinforcement, anchorage length, bond stress, slip

Temellerde Kolon Donatısının Basınç Aderansının Elastik-Plastik Analizi

Özet

Bu çalışmada kolon boyuna donatısının basınç aderansının elastik- plastik analizi sunulmuştur. Bu analizde beton ve çubuk arasındaki kayma gerilmelerinden doğan kayma kırılması göz önüne alınmıştır. Sonlu farklar hesabı ile birlikte Mindlin denklemine dayalı olarak, temelde ankraj boyunca aderans gerilmesi dağılımı, kolon çubuklarının yük-düşey yer değiştirme ilişkisi ve aderansın güç tükenmesine erişmesi için bağıntılar çıkarılmıştır. Teorik çözümlerin deney sonuçları ile iyi uyum içinde olduğu ve çubuğun relatif rijitliği K nın aderans gerilmesi dağılımını önemli ölçüde etkilediği gösterilmiştir.

Anahtar Sözcükler: Temel, nervürlü donatı, ankraj boyu, aderans gerilmesi, kayma

1. Introduction

The anchorage bond capacity of deformed bars is limited to one of two failure modes, namely, splitting failure (Ferguson and Thompson, 1962) and slip failure (Rehm, 1968). A large number of experiments have made it clear that bond failure of ribbed bars takes place by extensive splitting of the concrete cover due to inefficient containment. Typical examples are tensile lapped joints in beams (Roberts and Ho, 1973) and compression lapped joints in columns (Cairns and Arthur, 1979). Several researchers, such as Tepfers (1979) and Cairns (1979), have presented theoretical studies related to the splitting failure of concrete cover due to the radial component of bond forces exerted on the surrounding concrete from a ribbed bar.

In contrast, failure can occur by shearing of the concrete, i.e. slipping of the bar, provided that sufficient containment over the bar is present (Astill

and Al-Sajir, 1980; Astill and Turan, 1982) so that bursting forces produced by the bond action of the bar do not overcome the splitting resistance of the member prior to shearing forces. This type of bond failure was observed in tests concerning the anchorage bond of ribbed bars in the transference of load from columns to foundations, details of which are given in a previous study (Turan, 1983). This effect is related to the resistance to bursting forces provided by the large containment available over the column compression bars in the anchorage length of the base.

The Mindlin solution (Mindlin, 1936) for a force at a point in the interior of a semi-infinite elastic solid has led to the elastic analysis of many engineering problems associated with friction bonds (Mattes and Poulos, 1969; Poulos and Davis, 1968; Ivering, 1980). In the present study, the theoretical analysis of the compression bond of column longitudinal reinforcement in the foundation is carried out using the Mindlin equation (Mindlin, 1936) in conjunction with finite difference calculus, which takes into account slip failure of the ribbed bars in the anchorage lengths. The theoretical work is divided into two parts, namely, elastic analysis and elastic-plastic analysis.

2. Elastic Analysis

In this analysis, a cylindrical surface is assumed for ribbed bars with a nominal diameter of circular cross-section such that the bar configurations act as exaggerated roughness and the column longitudinal reinforcement is considered compressible in relation to the surrounding concrete with a constant elastic modulus E_s. The anchorage length of the bar is divided into n equal cylindrical elements. It is assumed that each bar element is subjected to a uniform bond stress. The bar tip is considered to be a smooth rigid circular disc of the same diameter as the bar shaft, across which a vertical stress is uniformly distributed and the embedding concrete medium is assumed to be an ideal elastic material with constant Young's modulus E_c and Poisson's ratio v_c.

The solution to the problem involves the computation of the displacement factors. The vertical displacement influence factors for the bar elements may be obtained by integration of the Mindlin equation (Mindlin, 1936). From the Mindlin equation the vertical displacement influence factor, at any point in a semi-infinite elastic solid, due to a downward force in the interior of the solid is

$$w_b = \frac{1}{16\pi G_c(1-v_c)}\left[\frac{3-4v_c}{R_1} + \frac{8(1-v_c)^2-(3-4v_c)}{R_2} + \frac{(\bar{z}-c)^2}{R_1^3} + \frac{(3-4v_c)(\bar{z}+c)^2-2c\bar{z}}{R_2^3} + \frac{6c\bar{z}(\bar{z}+c)}{R_2^5}\right] \quad (1)$$

where R_1, R_2, $\bar{z}$ and c are geometric relationships as shown in Figure 1, and R_1 and R_2 and are given by

$$R_1 = \sqrt{[\bar{r}^2+(\bar{z}-c)^2]}; \qquad R_2 = \sqrt{[\bar{r}^2+(\bar{z}+c)^2]} \quad (2)$$

As can be seen in Figure 2, $\bar{z} = (i-1/2), z = (\bar{z}+c)$ and $z_1 = (\bar{z}-c)$. Substituting $z = (\bar{z}+c), z_1 = (\bar{z}-c), \bar{z} = (z-c)$ and $G_c = E_c/(1+2v_c)$ in equation 1, and defining

$$V = \frac{1+v_c}{8\pi(1-v_c)E_c} \quad V_1 = \frac{z_1^2}{R_1^3} \quad V_2 = \frac{(3-4v_c)}{R_1}$$

$$V_3 = \frac{5-12v_c+8v_c^2}{R_2}$$

$$V_4 = \frac{(3-4v_c)z^2-2cz+2c^2}{R_2^3}$$

$$V_4 = \frac{6cz^2(z-c)}{R_2^5}$$

in which

$$R_1 = \sqrt{4a^2\cos^2\theta+z_1^2} \qquad R_2 = \sqrt{4a^2\cos^2\theta+z^2} \quad (3)$$

it follows that

$$w_b = V(V_1+V_2+V_3+V_4+V_5) \quad (4)$$

Referring to Figure 2, consider a point i at the mid-height of the ith element on the periphery of the bar having radius a. For the point i the influence factor for vertical displacement due to a bond stress on the jth element may be given by

$$w_{ij} = 4a\int_{(j-1)\delta}^{j\delta}\int_0^{\pi/2}[V(V_1+V_2+V_3+V_4+V_5)]d\theta dc \quad (5)$$

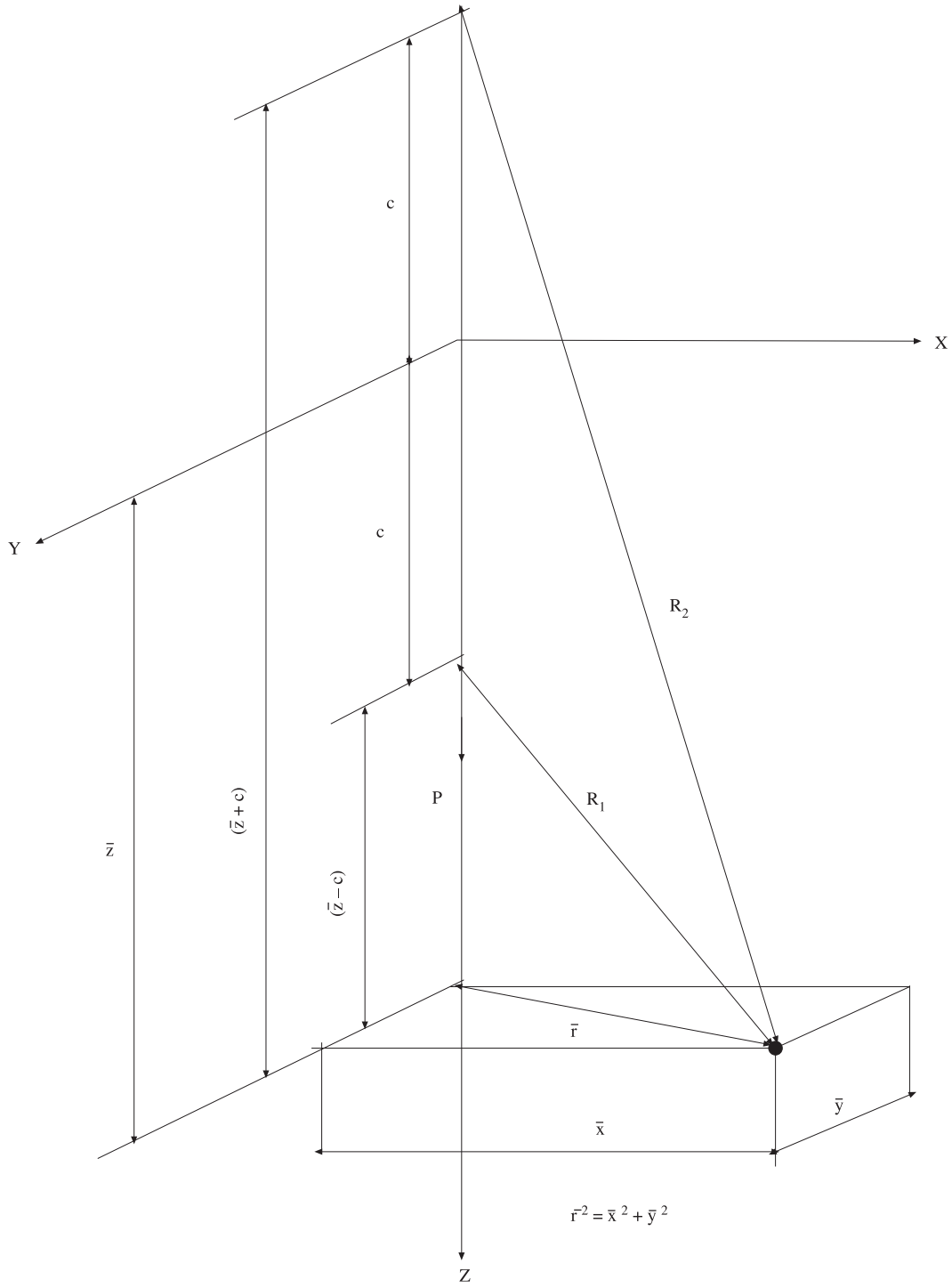

Figure 1. Geometric representation for Mindlin problem

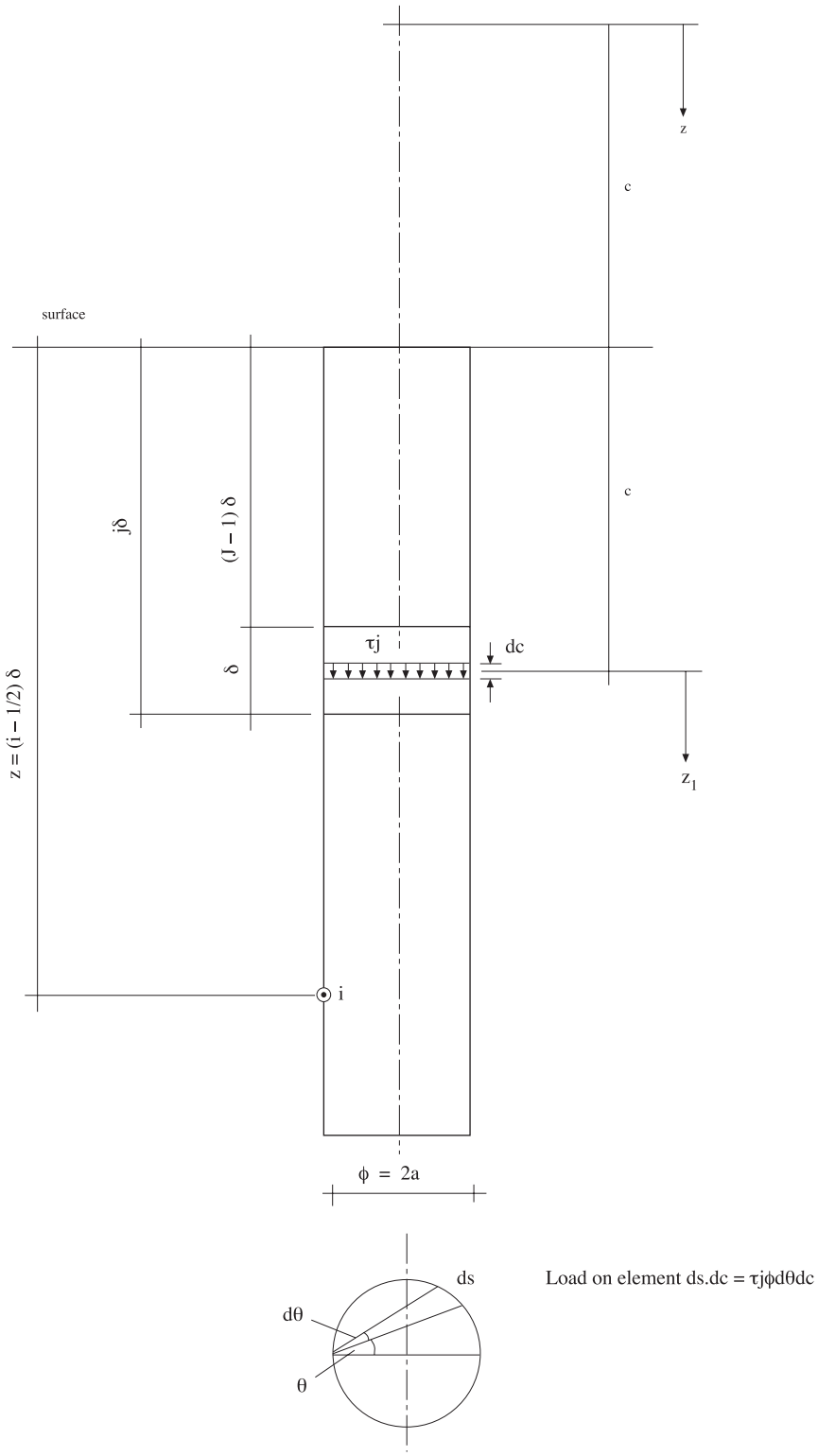

Figure 2. Geometric representation for a cylindrical bar element

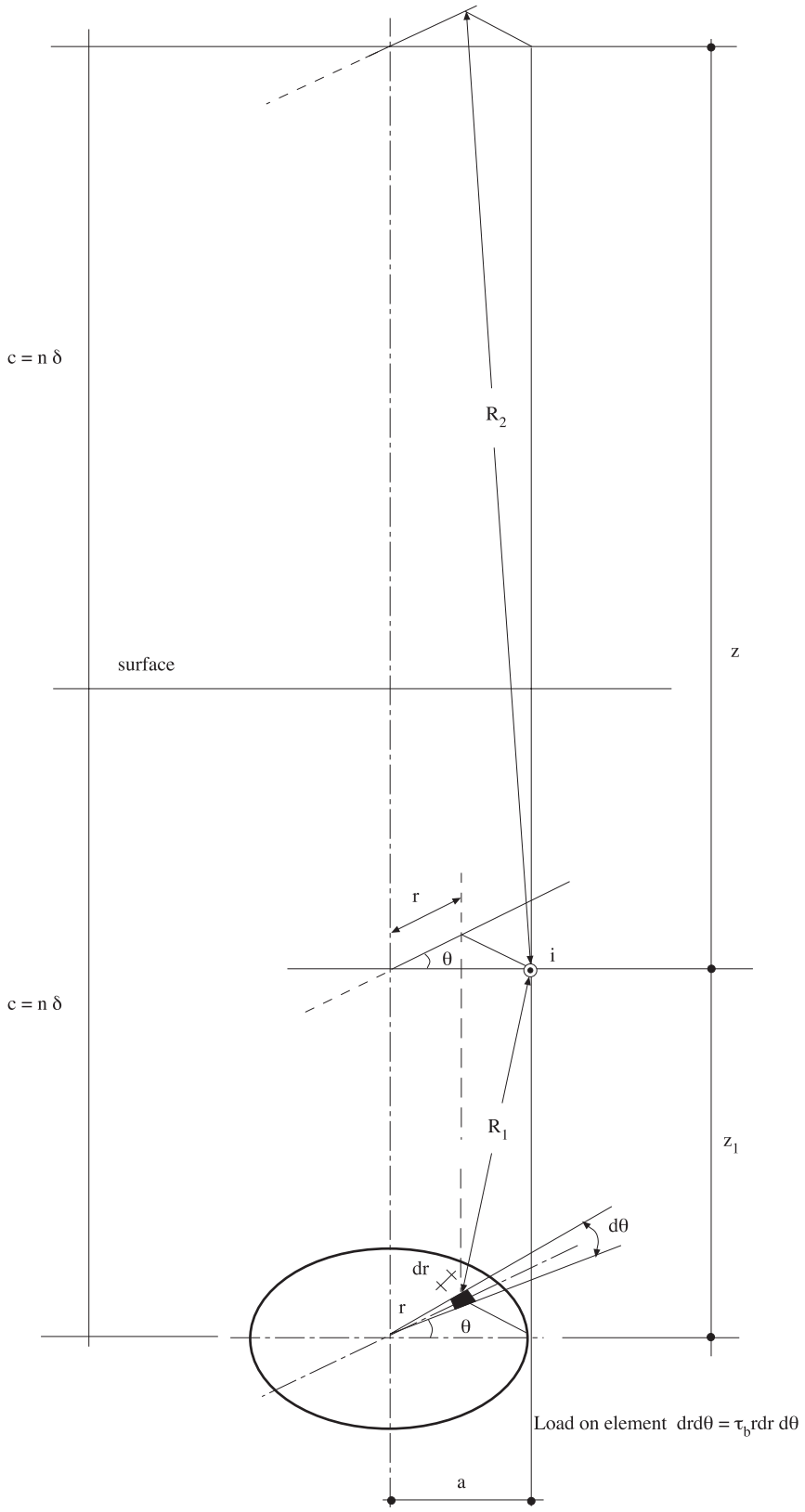

Figure 3. Geometric representation for the end of the bar

The geometric representation for the end of the bar (i.e. bar tip) is indicated in Figure 3. Similarly, for the point i the influence factor for vertical displacement due to uniform stress on the bar end is

$$w_{ib} = \int_0^{2\pi} \int_0^a [V(V_1 + V_2 + V_3 + V_4 + V_5)] r dr d\theta \quad (6)$$

in which

$$c = n; R_1 = \sqrt{z_1^2 + a^2 + r^2 - 2ra\cos\theta}; \\ R_2 = \sqrt{z^2 + a^2 + r^2 - 2ra\cos\theta} \quad (7)$$

If the influence factor for the displacement of the centre of the bar end due to bond stress on element j is taken into account, it will be

$$w_{bj} = 2\pi a \int_{(j-1)\delta}^{j\delta} [V(V_1 + V_2 + V_3 + V_4 + V_5)] dc \quad (8)$$

in which

$$i = n + \frac{1}{2}; R_1 = \sqrt{z_1^2 + a^2}; R_2 = \sqrt{z^2 + a^2} \quad (9)$$

Finally, the influence factor for vertical displacement of the bar tip due to the load on the tip is

$$w_{bb} = \frac{\pi^2}{2} \int_0^a [V(V_1 + V_2 + V_3 + V_4 + V_5)] r dr \quad (10)$$

For use in equation (10),

$$i = n + \frac{1}{2}; c = n; R_1 = r; R_2 = \sqrt{4c^2 + r^2} \quad (11)$$

The integrals in equations 5, 6, 7 and 10 are evaluated numerically. To carry out the numerical integration, the grid meshwork for the bar elements and the bar tip is shown in Figure 4. It is noted that the grid indication number M=49 was found to be satisfactory to produce sufficient accuracy in the numerical integrations, and was therefore used consistently throughout the theoretical analyses. The integration of equation 5 produces vertical displacement influence factors of all n elements of the bar due to a bond stress on each element, which may be given in matrix form as

$$[DB] = \begin{bmatrix} W_{11} & W_{11} & . & . & . & W_{ln} \\ W_{21} & W_{21} & . & . & . & W_{2n} \\ . & . & . & . & . & . \\ W_{n1} & W_{n1} & . & . & . & W_{mn} \end{bmatrix} \quad (12)$$

Likewise, the integration of equation 5 produces vertical displacement influence factors for n bar elements due to a normal stress on the bar tip. Similarly, the integration of equation 8 yields the displacement influence factors for the bar tip due to a bond stress on n elements of the bar. They may be expressed by the following column and row matrices respectively.

$$[DC] = \begin{bmatrix} W_{1b} \\ W_{2b} \\ \\ . \\ W_{nb} \end{bmatrix} \quad (13)$$

$$[DF] = \begin{bmatrix} W_{b1} & W_{b2} & . & . & W_{bn} \end{bmatrix} \quad (14)$$

Finally, the integration of equation 10 yields a scalar representing the displacement influence factor for the bar tip itself, which is labelled as

$$W_{bb} = W_{bb} \quad (15)$$

Expressions 12, 13, 14, and 15 may be collected in an overall matrix given by

$$[CS] = \begin{bmatrix} W_{11} & W_{12} & . & . & . & W_{ln} & W_{1b} \\ W_{21} & W_{22} & . & . & . & W_{2n} & W_{2b} \\ . & . & . & . & . & . & \\ W_{n1} & W_{n2} & . & . & . & W_{nm} & W_{nb} \\ W_{b1} & W_{b2} & . & . & . & W_{bn} & W_{bb} \end{bmatrix} \quad (16)$$

It is noted that when the end bearing of the bar is neglected, matrix [CS] becomes

$$[CS] = [DB] \quad (17)$$

3. Proposed Method

An outline of a cylindrical bar of length (l_a) embedded in an isotropic elastic concrete medium is shown in Figure 5. Since the elastic conditions prevail in the surrounding concrete, at any point along the bar periphery the displacements of the concrete must be compatible to those of the bar itself. Thus, to obtain a solution for the unknown stresses on the bar-to-concrete interface and the corresponding displacements, the displacement of the concrete adjacent to the bar may be equated to the displacement of the bar itself.

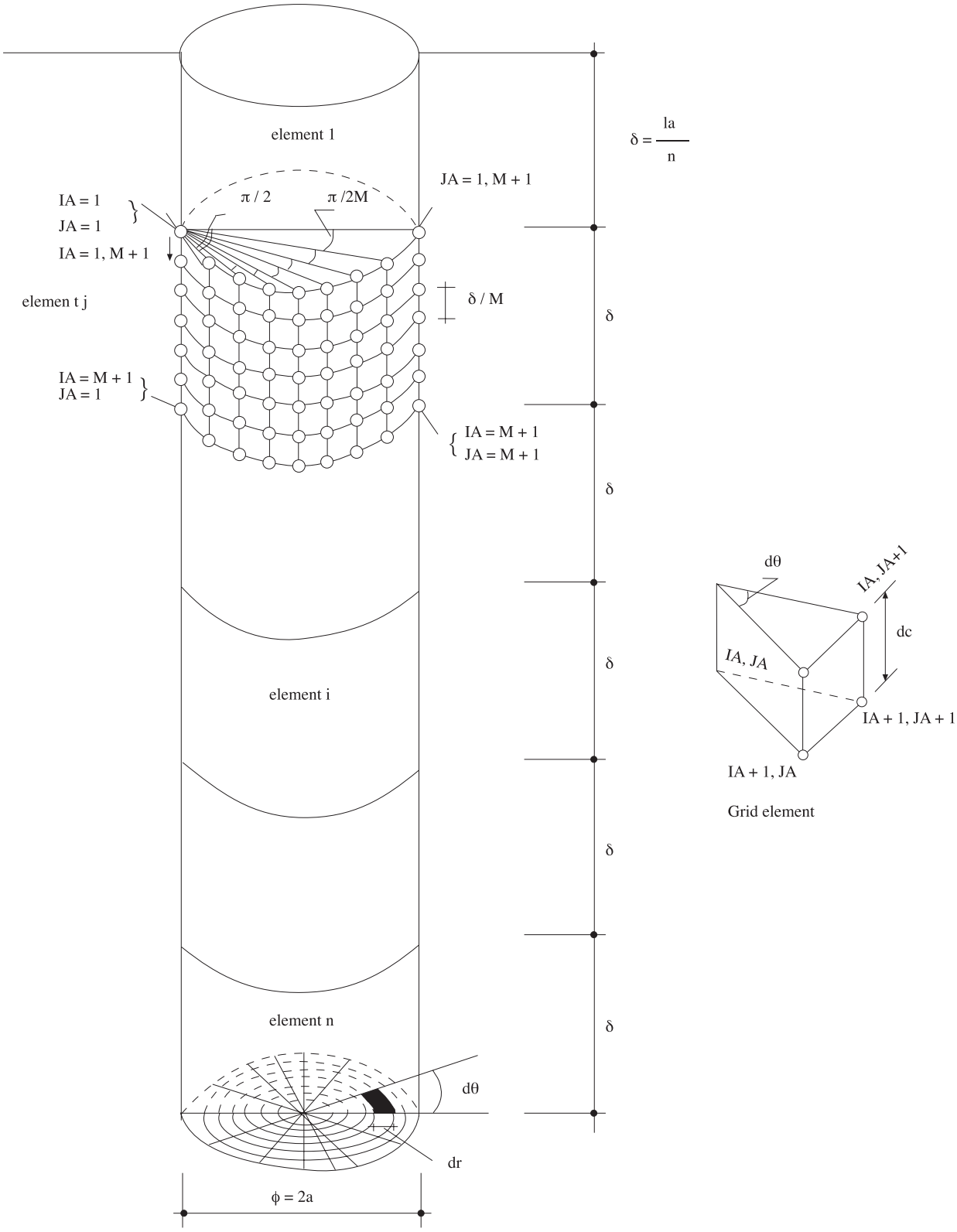

Figure 4. Grid meshwork of bar elements and the bar tip

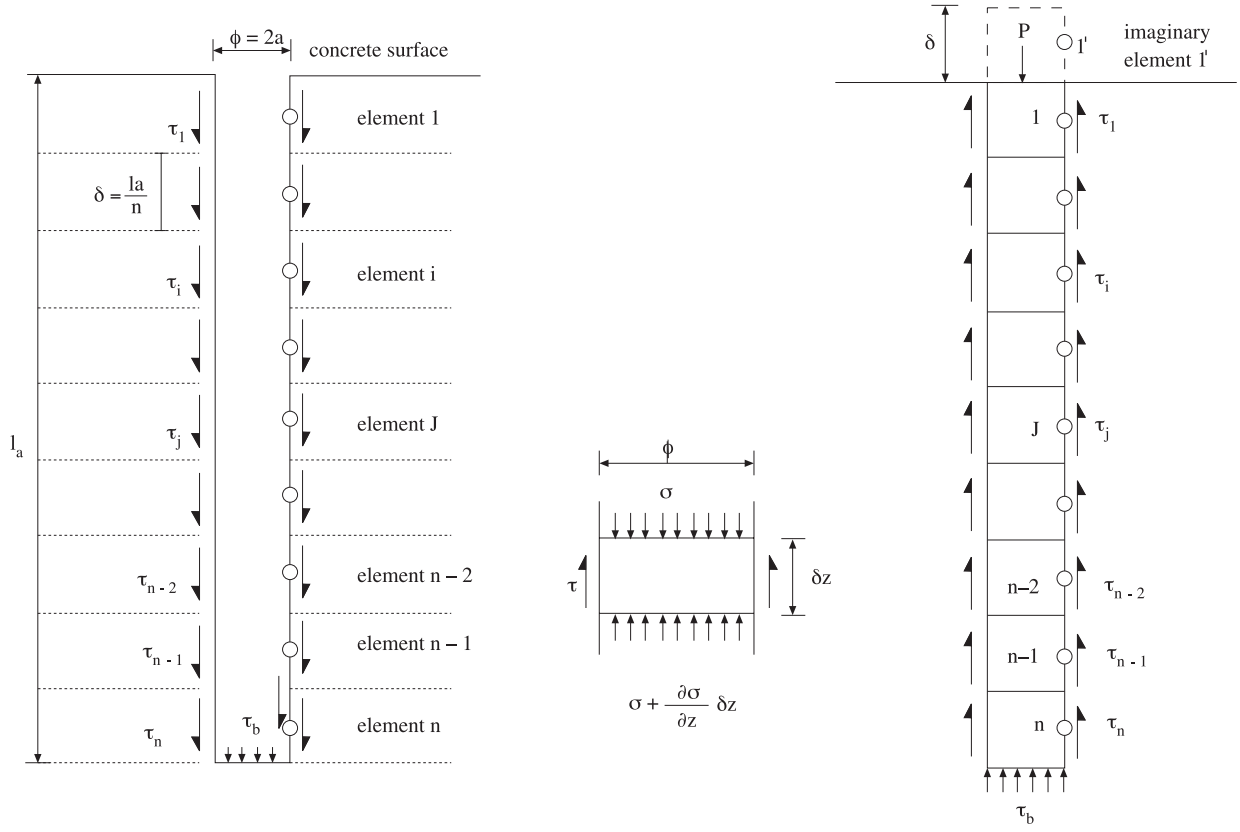

a) Interaction stresses on the bar – concrete interface

b) Stresses in a small cylin drical element of the bar

c) Stresses acting on the bar

Figure 5. Stresses in the bar and surrounding concrete medium

It was evident from previous tests (Turan, 1983) that the bursting forces produced by the bond action of the ribbed bars were ineffective because of the large concrete containment available over the bars in the base. On the other hand, inclusion of base tension reinforcement - which is normally always present - or provision of links round the bars within the anchorage length, or a combination of the two also introduces an extra confining element to the bars against the bursting effect. Thus, the bursting forces are virtually negligible in the foundation, and, hence the radial displacement of the concrete is very small. Therefore, the radial displacement of the concrete is neglected in the analysis, and only the compatibility of the vertical displacement is taken into account. The vertical displacements are computed at the mid-point of the periphery of each bar element.

Referring to Figure 5a, let the vertical displacement of the concrete adjacent to the bar at any element i, due to a bond stress on element j, be Δc_{ij}. Taking downward displacement to be positive, Δc_{ij} may be given by

$$\Delta c_{ij} = \frac{\phi}{E_c} W_{ij} \tau_{ij} \tag{18}$$

Similarly, the displacement at i due to a normal stress on the bar tip is

$$\Delta c_{ib} = \frac{\phi}{E_c} W_{ib} \tau_{ib} \tag{19}$$

Thus, the vertical displacement at i due to all n bar elements and to the bar tip may be expressed as

$$\Delta c_i = \frac{\phi}{E_c} \left(\sum_{j=1}^{n} W_{ij} \tau_{ij} + W_{ib} \tau_{ib} \right) \tag{20}$$

When the vertical displacement of the concrete under the bar tip due to the bond stress on element j is considered, it will be

$$\Delta c_{bj} = \frac{\phi}{E_c} W_{bj} \tau_j \tag{21}$$

Finally, the vertical displacement of the concrete under the bar tip due the normal stress on the bar tip may be expressed as

$$\Delta c_{bb} = \frac{\phi}{E_c} W_{bb} \tau_b \tag{22}$$

Hence, the vertical displacement of the concrete under the bar tip due to all n bar elements and to the bar tip itself is

$$\Delta c_b = \frac{\phi}{E_c} (\sum_{j=1}^{n} W_{bj} \tau_j + W_{bb} \tau_b) \tag{23}$$

Equations 20 and 23 may be formulated in the following matrix form:

$$[\Delta c] = \frac{\phi}{E_c} [CS][\tau] \tag{24}$$

In order to determine the displacement of the bar itself, the bar is assumed to be subjected to pure axial compression only. Consider a small bar element on which the stresses act as shown in Figure 5b. From the vertical equilibrium of the bar element, resolving forces leads to the following expression

$$\frac{\partial \sigma}{\partial z} = -\frac{\tau \pi \phi}{A_s} \tag{25}$$

Defining A_s as

$$As = \frac{\pi \phi^2}{4} \tag{26}$$

and substituting A_s in equation 26 and simplifying gives

$$\frac{\partial \sigma}{\partial z} = -\frac{4\tau}{\phi} \tag{27}$$

Referring to Figure 5b, consideration of the axial strain of the bar element gives

$$\frac{\partial \Delta s}{\partial z} = -\frac{\sigma}{E_s} \tag{28}$$

where Δs is the displacement of the bar. Differentiating equation 18 with respect to z and substituting $\partial\sigma/\partial z$ from equation 27 leads to the following equation for the displacement of the bar:

$$\frac{\partial^2 \Delta s}{\partial z^2} = \frac{4\tau}{\phi E_s} \tag{29}$$

Equation 29 may be represented in terms of the finite difference expressions. For an element i within the interval $n - 1 \geq i \geq 2$, equation 19 may be expressed in the following finite difference form to give the bond stress as

$$\tau_i = \frac{\phi}{4\delta^2} E_s (\Delta s_{i-1} - 2\Delta s_i + \Delta s_{i+1}) \tag{30}$$

$\Delta s_{i-1}, \Delta s_i$ and Δs_{i+1} are the displacements of the mid-points of the elements i-1, i and i+1 respectively, and $\delta = l_a/\mathrm{n}$

Referring to Figure 5c, at the top of the bar consider an imaginary element having a mid-point displacement $\Delta' s_1$, above the first real element. At the top of the bar, the normal stress in the bar is

$$G = \frac{P}{A_s} \tag{31}$$

Hence, referring to equation 28, the displacement of the imaginary element may be related to the displacement of the uppermost real element as

$$\Delta' s_1 = \Delta s_1 + \frac{\sigma}{E_s} \tag{32}$$

Substituting 31 in equation 32, re-writing equation 30 for the first real element and substituting the value of $\Delta'\ s_1$ from 32 in equation 30 results in the bond stress on the first element in the form

$$\tau_1 = \frac{\phi}{4\delta^2} E_s (-\Delta s_1 + \Delta s_2) + \frac{Pn}{\pi \phi l_a} \tag{33}$$

In order to obtain the finite difference expression for the bottom element of the bar n, the bond stress may be related to the displacements of elements n-2, n-1, n and the bar tip, using equation 29 and finite differences for points with unequal spacing, which yields the required expression for the bond stress on the element n as follows:

$$\tau_n = \frac{\phi}{4\delta^2} E_s (-0.2\Delta s_{n-2} + 2\Delta s_{n-1} - 5\Delta s_n + 3.2\Delta s_b) \tag{34}$$

Finally, to obtain the expression for the bar tip, i.e. the (n+1)th element, equation 28 may be applied to the bar tip, employing a finite difference expression for an unequal spacing of pivotal points, which leads to

$$\tau_b = \frac{\phi}{4\delta^2} E_s \frac{l_a}{\phi n} (-1.33\Delta s_{n-1} + 12\Delta s_n - 10.67\Delta s_b) \tag{35}$$

Equations 30, 33, 34 and 35 may be given in matrix form as

$$[\tau] = \frac{\phi}{4\delta^2} E_s [CP][\Delta s] + [Y] \tag{36}$$

where [CP] is the (n+1) square matrix of coefficients for bar action and is defined by

$$[CP] = \begin{bmatrix} -1 & 1 & 0 & 0 & . & . & . & 0 & 0 & 0 & 0 \\ 1 & -2 & 1 & 0 & . & . & . & 0 & 0 & 0 & 0 \\ 0 & 1 & -2 & 1 & . & . & . & 0 & 0 & 0 & 0 \\ . & . & . & . & . & . & . & . & . & . & . \\ 0 & 0 & 0 & 0 & . & . & . & -0.2 & 2 & -5 & 3.2 \\ & & & & . & . & . & 0 & -1.33t & 12t & -10.67t \end{bmatrix} \tag{37}$$

in which

$$t = \frac{l_a}{\phi n} \tag{38}$$

$[\Delta s]$ and [Y] are the (n+1) column matrices defined by

$$[\Delta s] = \begin{bmatrix} \Delta s_1 \\ \Delta s_2 \\ . \\ \Delta s_n \\ \Delta s_b \end{bmatrix} \tag{39}$$

$$[Y] = \begin{bmatrix} \frac{Pn}{\pi \phi l_a} \\ 0 \\ . \\ . \\ . \end{bmatrix} \tag{40}$$

Since the conditions within the concrete remain elastic, the displacements of the concrete and the bar must be compatible.
Hence

$$[\Delta s] = [\Delta c] \tag{41}$$

From equations 14 and 26,

$$[\tau] = \left([I] - \phi^2 \frac{E_s}{4\delta^2 E_c} [CP][CS] \right)^{-1} [Y] \tag{42}$$

where [I] is the identity matrix. Defining

$$K = \frac{E_s}{E_c} \tag{43}$$

$$\delta = \frac{l_a}{n} \tag{44}$$

and

$$[C] = [I] - \frac{n^2}{4\left(\frac{l_a}{\phi}\right)^2} K[CP][CS] \tag{45}$$

it follows that

$$[\tau] = [C]^{-1}[Y] \tag{46}$$

Solution of equation 45 produces unknown bond stress on the bar surface along the anchorage length of base and the normal stress acting on the bar tip, or, in the case of no end bearing, bond stresses on the bar periphery only. Then the distribution of displacement along the bar can be computed from equation 14. The elastic analysis is extended in order to carry out elastic-plastic analysis by considering the local bond failure between the reinforcing bar and surrounding concrete medium.

4. Elastic-Plastic Analysis

For the development of the elastic-plastic analysis, a uniform and constant ultimate bond strength is considered for each bar element along the anchorage length, and a uniform ultimate end bearing resistance for the bar tip when the end bearing is present. It is assumed that when the bond stress developed on any bar element reaches the ultimate bond strength, local yield (i.e. bond failure) will occur in the related concrete layer, and, therefore, displacement compatibility does not exist between the bar element and, this concrete layer, while the rest of the concrete layers remain elastic.

Consider a bar with n elements embedded in a concrete medium and subjected to an axial load as shown in Figure 6a. The corresponding stresses are indicated in Figure 6b. As the externally applied load increases, the stresses and displacements increase proportionally until the bond stress somewhere on a bar element reaches ultimate bond strength in the related concrete layer. Once this occurs, the layer is not compatible with the bar element concerned. The displacements and bond stresses elsewhere in the bar now increase at a faster rate because any increase in the applied load will cause a redistribution of stresses and displacements in the remaining elastic layers. The ultimate bond stress on the element, however, preserves its value, as seen in Figure 6c. This continues until the ultimate stresses on all bar elements develop in the related concrete layers as shown in Figure 6d the failure takes place in the foundation. The steps for the elastic-plastic analysis are given as follows:

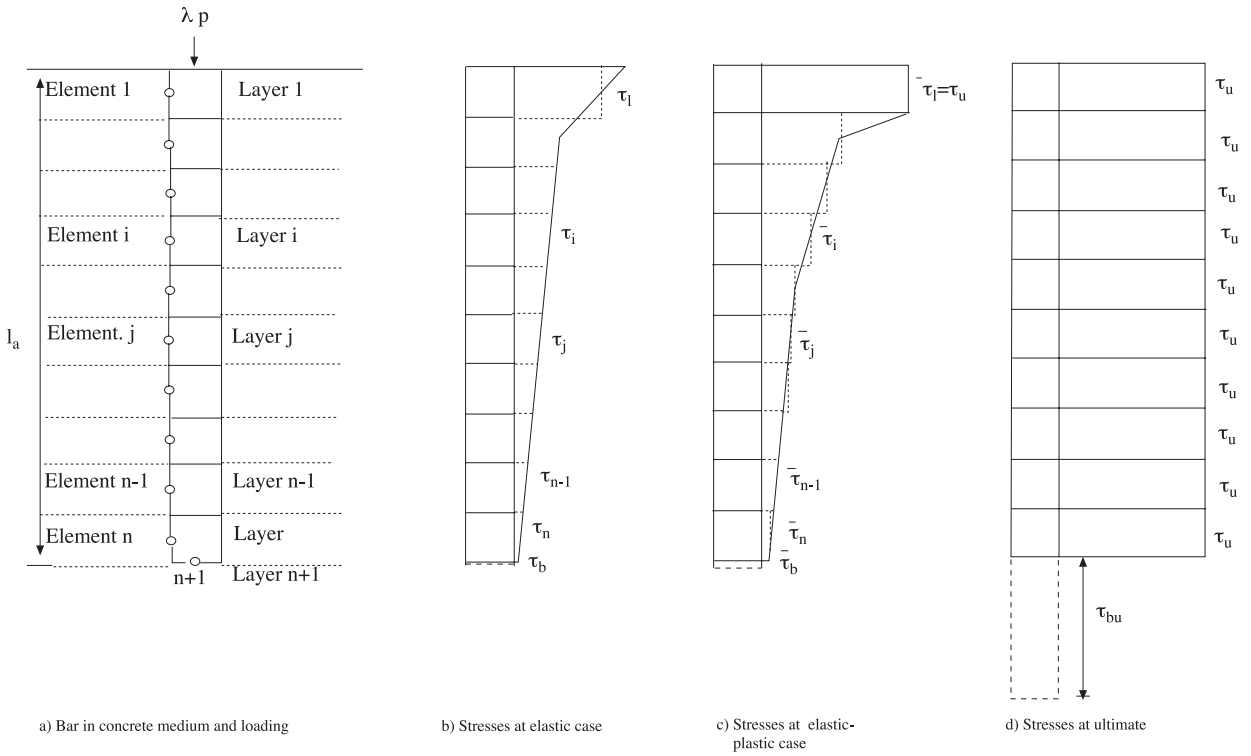

Figure 6. Geometric representation for elastic-plastic analysis

1- The reinforcing bar is analysed elastically once under [C] and [Y] for an axial working load of p. The resulting bond stresses on the bar shaft and the associated vertical displacements, or, in the case of end bearing, the bond stresses on the bar periphery together with the normal stress on the bar tip and the corresponding displacements are computed. For convenience they are stored in the column matrices [ST] and [DEF], respectively:

$$[ST] = \begin{bmatrix} \bar{\tau}_1 \\ \bar{\tau}_2 \\ . \\ \bar{\tau}_n \\ \bar{\tau}_b \end{bmatrix} \tag{47}$$

$$[DEF] = \begin{bmatrix} \bar{\Delta}c_1 \\ \bar{\Delta}c_2 \\ . \\ \bar{\Delta}c_n \\ \bar{\Delta}c_b \end{bmatrix} \tag{48}$$

2- Every possible yield location within the concrete layers due to the ultimate bond stress on the related bar element is taken into consideration in turn, and the load factor at which local yield occurs in the concrete layer k is computed from

$$\lambda_1^k = \frac{\tau_u^k}{\bar{\tau}_k} \tag{49}$$

where τ_u^k is the ultimate bond strength of the bar in layer k and $\bar{\tau}_k$ is the bond stress on the bar element in layer k due to the applied working load. The lowest of these predicted load factors is chosen. This is now the load factor λ_1 at which the first yield occurs in layer k*. The current stresses on the bar elements and displacements are obtained by scalar multiplying the column matrices [ST] and [DEF] by λ_1. Since the layer k* has yielded, the free slip of the bar occurs in this layer. After that, any increase in the applied load will lead to a redistribution of stress on the bar elements in the remaining layers. Therefore, the displacement compatibility between the bar and the concrete in the elastic layers must be considered. Then the resulting compatibility equations are solved in order to obtained the distribution of stress and displacement along the bar until the yield of the next concrete layer takes place.

3- For a further increase $\Delta\lambda = \lambda - \lambda_1$ in the load factor, the current stresses and displacements

are calculated as

$$[ST]^{\lambda} = [ST]^{\lambda_1} + \Delta\lambda[\tau] \tag{50}$$

$$[DEF]^{\lambda} = [DEF]^{\lambda_1} + \Delta\lambda[\Delta c] \tag{51}$$

where $[ST]^{\lambda}$ represents the bond stresses or bond stresses and normal stress under the load parameter λ, while $[ST]^{\lambda_1}$ relates the same stresses under load factor λ_1. Similarly $[DEF]^{\lambda}$ and $[DEF]^{\lambda_1}$ represent the vertical displacements under the load factors λ and λ_1 respectively. Again, each yield location in the concrete layers is considered in turn. The load factor at which a local yield occurs in that layer is calculated by equating the current bond stress to the ultimate bond strength of the layer. Thus,

$$\lambda_2 = \lambda_1 + \frac{\tau_u(i) - ST(i)}{\bar{\tau}(i)} \tag{52}$$

The smallest of these load factors is selected as the load factor which causes the next yield in one of the concrete layers. The bar stiffness factor K is very small, i.e. the bar is compressible in relation to the surrounding concrete, and, therefore, high bond stresses develop at the top on the surface of the first bar element, as shown in Figure 6b. Consequently, the yield starts at the top of the bar in the first concrete layer and continues progressively downward in the remaining elastic layers towards the bottom as the applied load is increased.

4- The current stresses on the bar elements and the associated vertical displacements are computed from equations 50 and 51 by substituting $\Delta\lambda = \lambda_2 - \lambda_1$ and $\Delta\alpha = \lambda_2$. If all the concrete layers have yielded due to the ultimate bond stress development on the bar elements and the ultimate bearing resistance of the concrete under the bar tip has been attained when the end bearing is present, the process is stopped. Otherwise, λ_2 is taken as λ_1 and the steps 2 and 3 are repeated until failure takes place. To assess the ultimate bond strength for the bar elements along the anchorage length, the expressions obtained from a regression analysis of the test results, details of which are given in a previous study (Turan, 1983), are used.

5. Bond Stress Distribution

To simulate the conditions in the tests and for direct comparison, the end bearing of the column bars was not considered in the solutions for the prediction of bond stress distribution with load. Figure 7 shows the theoretical and experimental load-bond stress distribution curves in test SR2-1, which used 4-25 mm ribbed bars in a plain concrete base. The bar stiffness factor, which is the measure of compressibility of the bar, is very small, i.e. K=Es/Ec=7.74, in the test. The theoretical analysis therefore shows that the bond stress is greatest on the first bar element and least on the last element in the anchorage length. This is the general trend observed experimentally in tests conducted on full-scale bases (Turan, 1983), in which the bar stiffness factor K varied between 6.76 and 9.90. In the elastic stage, the theoretical bond stress is slightly higher than the experimental one at the top and bottom part of the anchorage length, while the experimental value of the bond stress is slightly higher than the theoretical value in the middle part up to a load of 140 kN. Beyond this load, the discrepancy between the values at the top and middle parts of the anchorage length gradually increases. At a load of 360 kN, where the theoretical bond stress has reached the ultimate value on two bar elements, the theoretical curve indicates higher values in the upper part and lower values in the lower part of the anchorage length than those recorded in the experimental curve. The mean value of the ratio of the theoretical bond stress to the experimental bond stress for all bar elements is 0.975. At a load of 490 kN, both curves indicate closer agreement and, the mean value of ratio of the theoretical bond stress to experimental bond stress is 0.992. Finally, at a load of 560 kN, beyond which no more experimental data was available due to the first effective slip, both curves are in close agreement. At the lower part of the anchorage length, both curves agree approximately, while the experimental curve indicates a peak at the top. It can also be seen in Figure 7 that on both curves bond stresses decrease to a very small magnitude at approximately the same location at the bottom part of the anchorage length. This effect was also observed by Ivering (1980) in the elastic analysis of tube anchorage in rock.

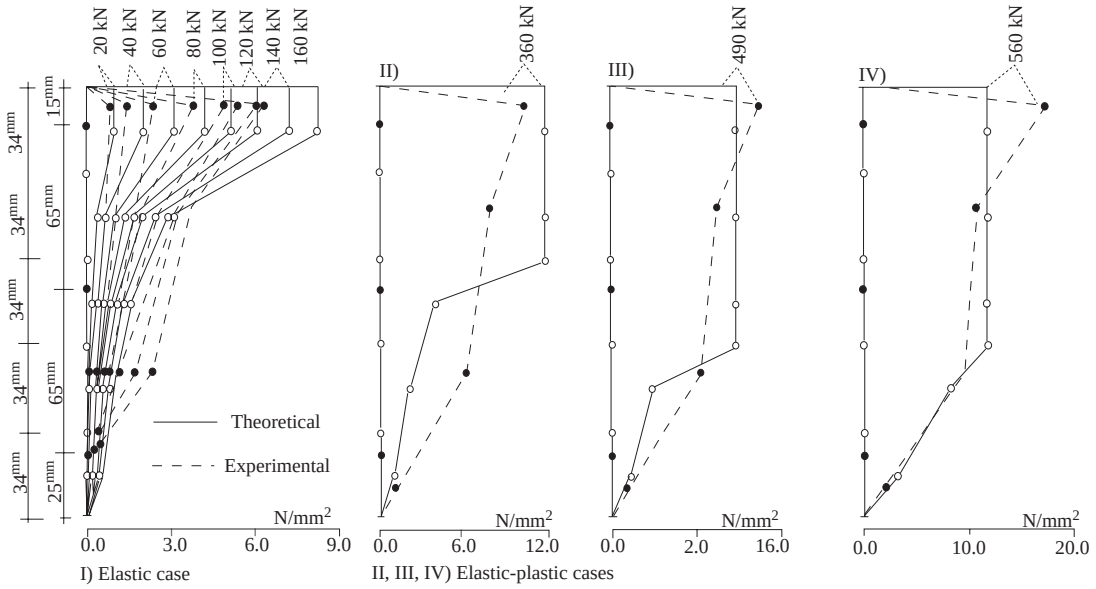

Figure 7. Load versus experimental and theoretical bond stress distribution in test SR 2.

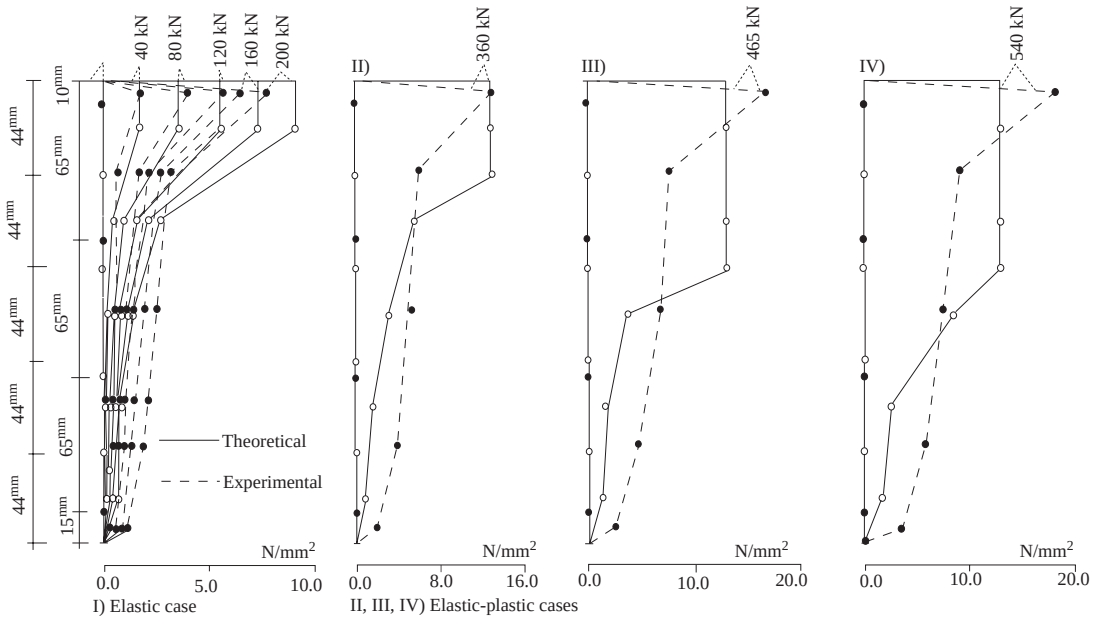

Figure 8. Load versus experimental and theoretical bond stress distribution in test SR 2-2

Figure 8 shows load versus theoretical and experimental bond stress distributions for test SR2-2, which varies the anchorage length of column bars in the base. The theoretical and experimental curves indicate that the bond stress is greatest at the top and least in the bottom region of the anchorage length. In the elastic stage, there is close agreement with the theoretical curve, the experimental curve records slightly greater bond stresses in the top and slightly smaller bond stresses at the bottom part of the base up to a load of 160 kN. After this level of load the theoretical values are greater in the upper part, while the experimental values increase at a higher rate in the lower part of the anchorage length. The theoretical and experimental bond stress curves are illustrated in Figure 8 for the loads of 360 kN, 465 kN and 540 kN respectively, the final load being the load beyond which no experimental data was

available due to the first slip. The mean ratio of the theoretical bond stress to the experimental bond stress is 0.977, 0.985 and 0.988 respectively for these loads.

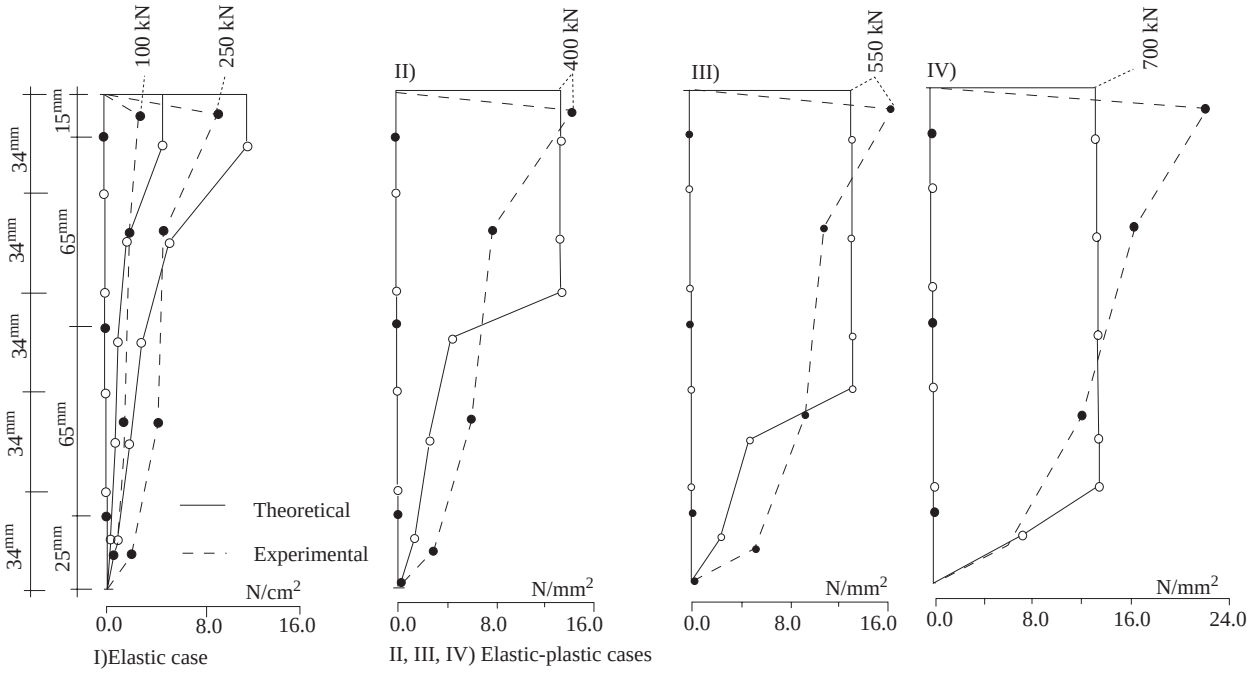

Figure 9. Load versus experimental and theoretical bond stress distribution in test SR7-1

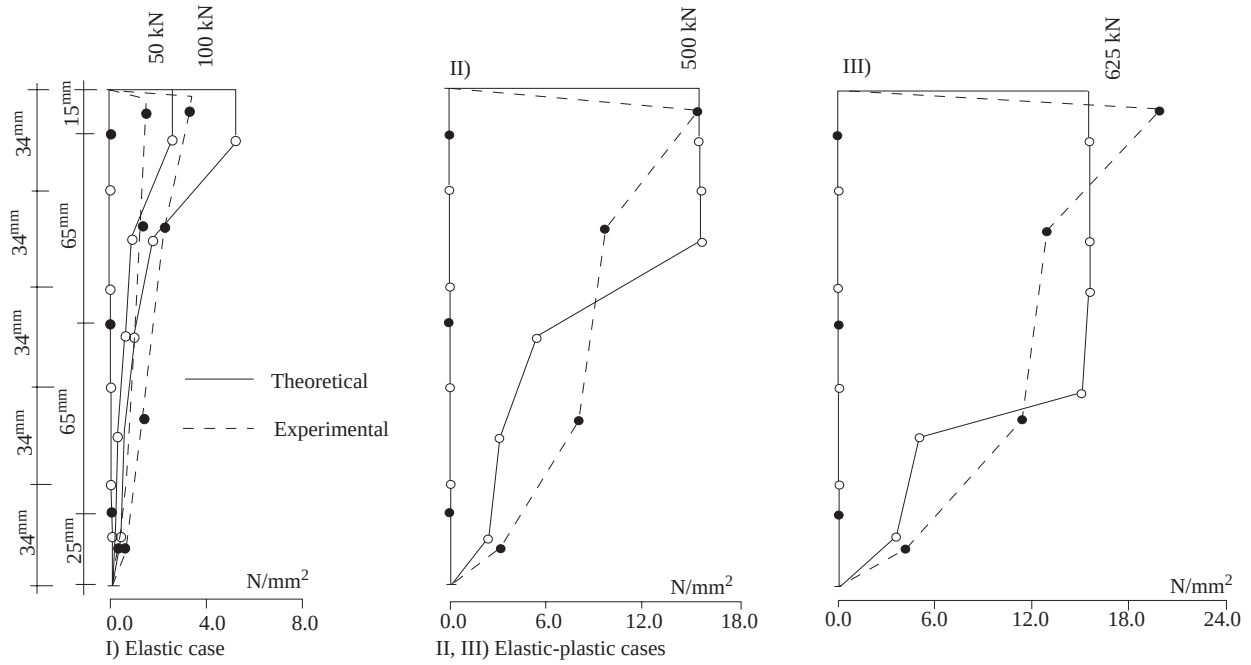

Figure 10. Load versus experimental and theoretical bond stress distribution in test SR7-2

Figure 9 shows the theoretical and experimental load-bond stress distribution curves for test SR7-1, which includes closely spaced links over the column bars in the base. In the elastic stage both curves descend nonlinearly towards the bottom of the base and show similarities in shape. However, the theoretical curve indicates higher values at the top and lower values at the bottom part of the anchorage length than those recorded by the experimental curves. In the elastic-plastic stage, the theoretical and experimental curves are shown at loads of 400 kN, 550 kN and 700 kN respectively, the final load being the load stage beyond which experimental data was not obtainable due to the first slip. The mean ratio of the theoretical bond stress to the experimental bond stress indicated by the curves is 0.992, 0.975 and 1.022 at loads of 400 kN, 550 kN and 700 kN respectively.

Figure 10 shows a series of theoretical and experimental load-bond stress distribution curves for test SR7-2, in which transverse reinforcement is introduced. Both curves indicate that the maximum bond stress is at the top near the column to base interface at each load step until the first slip occurs. Both curves also show that the maximum bond stress at the top decreases downward and reaches the lowest level at the bottom part of the anchorage length. In the elastic stage, the experimental curve records smaller values at the upper part and higher values at the lower part of the base than those indicated by the theoretical curve. In the elastic-plastic stage, the theoretical and experimental bond stress curves are also shown at loads of 500 kN and 625 kN, the latter being the load beyond which the first slip occurred. The mean value of the ratio of the theoretical bond stress to the experimental bond stress for the above loads is 0.973 and 0.978 respectively.

In the remainder of the 16 tests, the theoretical bond stress distribution along the anchorage length follows the same trend as that described in the preceding paragraphs. From the above observations it is concluded that the proposed theory predicts the bond stress distribution with reasonable accuracy by comparison with the experimental results. The bar stiffness factor K has a significant influence on the distribution of bond stress and, as K decreases, the magnitude of the bond stress at the top part of the anchorage length increases.

By considering the end bearing of the bar, a separate series of theoretical computations were carried out. These solutions showed that the distribution of bond stress along the anchorage length was not materially different from that of distribution without end bearing. This can be attributed to the low bar stiffness factor K, such that only small stresses develop at the bottom part of the bar, including the normal stress on the bar tip. Consequently, a small proportion of the load would be transferred to the concrete by the end of the bar. This effect was also observed by Mattes and Poulos (1969) for compressible piles. However, to clarify this, further experimental and theoretical studies are required.

6. Vertical Displacements

To obtain the theoretical values, the anchorage length of the bar was divided into ten equal elements, and then elastic-plastic analysis without end bearing was carried out. The vertical displacement of the column bars at each yield of concrete layer in the base was computed as

$$\Delta_{sv} = \frac{\lambda^i p(\delta i + l_v)}{A_s E_s} + (DEF)_i \tag{53}$$

where the first term on the right hand side indicates the vertical displacement of the column bars itself in axial compression at load factor λ^i, which comprises the length of bar elements (δ.1) within the yielded concrete layers and the length of the column bars l_u above the base, and $(\mathrm{DEF})_i$ is the vertical displacement of the concrete obtained from equation 14 at load factor λ^i.

Figure 11 shows the theoretical and experimental vertical displacements plotted against the applied load for test SR2-1. It can be seen that neither curve shows any significant change and they almost match each other near the ultimate load. Up to a level of two-thirds of the experimental failure load, the experimental curve is slightly steeper than the theoretical one. Beyond this stage the theoretical curve becomes steeper as the experimental curve diverges close to the failure. However, the values indicated by the experimental curve are insignificantly different in numerical terms from the theoretical values. Finally, the experimental curve records a very large amount of slippage, indicating the failure of the test. At the ultimate load, the theoretical curve also shows that as the displacement compatibility is lost between the steel and concrete, due to the ultimate bond stress development on the bar shaft, full slip takes place in the base.

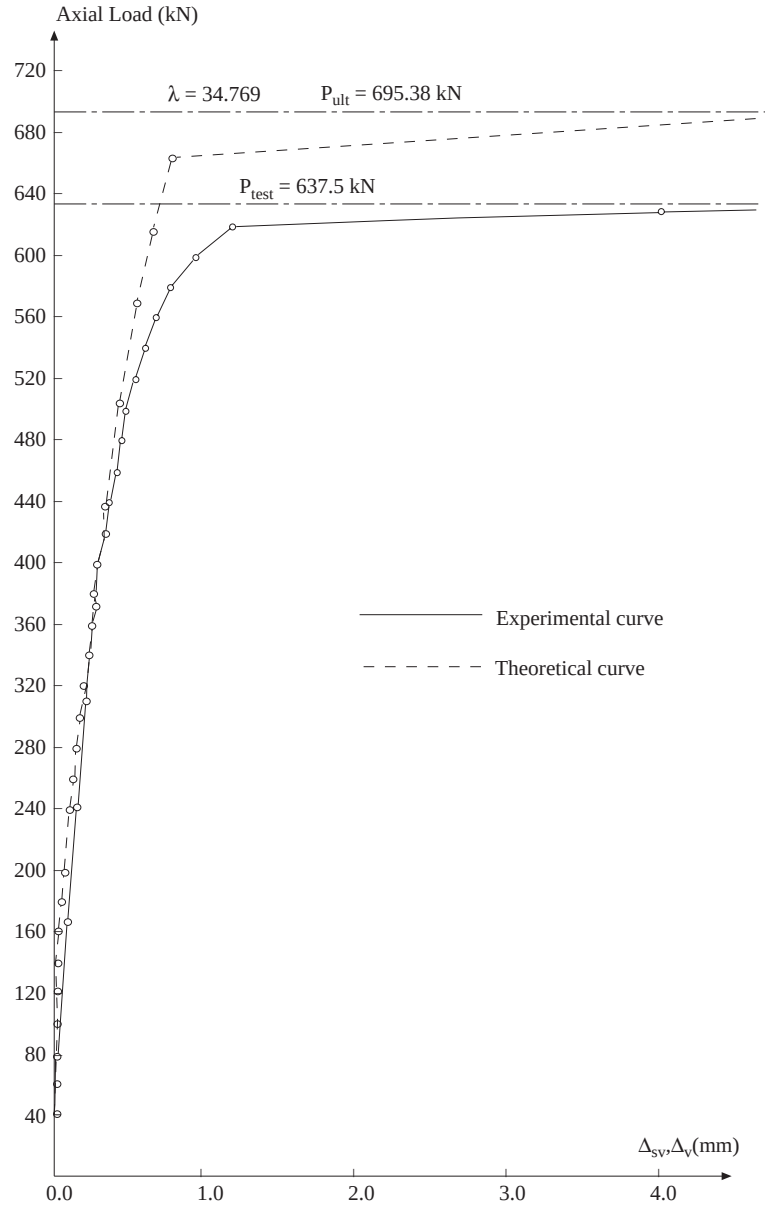

Figure 11. Theoretical and experimental load-vertical displacement curves for test SR2-1

A comparison of the theoretical and experimental load-vertical displacement diagrams for test SR2-2 is shown in Figure 12. The theoretical curve indicates slightly overestimated values compared with the experimental curve up to approximately 60% of the experimental load. Beyond this stage, the experimental curve becomes gradually flatter with loading, but the displacements are relatively small close to the failure. Eventually, the curve shows that major slip takes place at the ultimate load. The theoretical curve also shows that as the failure load is approached full slip occurs in the anchorage length of the base.

Figure 13 shows the theoretical and experimental load-vertical displacement curves for the column bars in test SR7-1. Both curves almost match each other, the experimental curve being slightly steeper than the theoretical one, up to approximately two-thirds of the failure load. Then the experimental curve gradually diverges close to the failure. The experimental curve also shows that major slip takes place at the ultimate load. When the theoretical fail-

ure load is approached full slip of the column bars in the anchorage length takes place.

Figure 14 indicates the theoretical and experimental vertical displacement of the column bars with respect to the applied load for test SR7-2. It can be seen that both curves agree without any significant change, from zero to nearly half the ultimate load. Then, the theoretical curve becomes steeper as the experimental curve gradually diverges with loading. However, the difference between the theoretical and experimental values is not significant near to the ultimate load. Finally, both curves indicate that full slip of the bars occurs in the anchorage length of the base at the ultimate load.

7. Ultimate Loads

A comparison of the theoretical and experimental failure loads for the foundation tests is given in Table 1. For direct comparison with the experimental failure loads, the end bearing of the column bars was neglected in the analysis. The ultimate load of the tests, which used four column bars throughout, was computed as

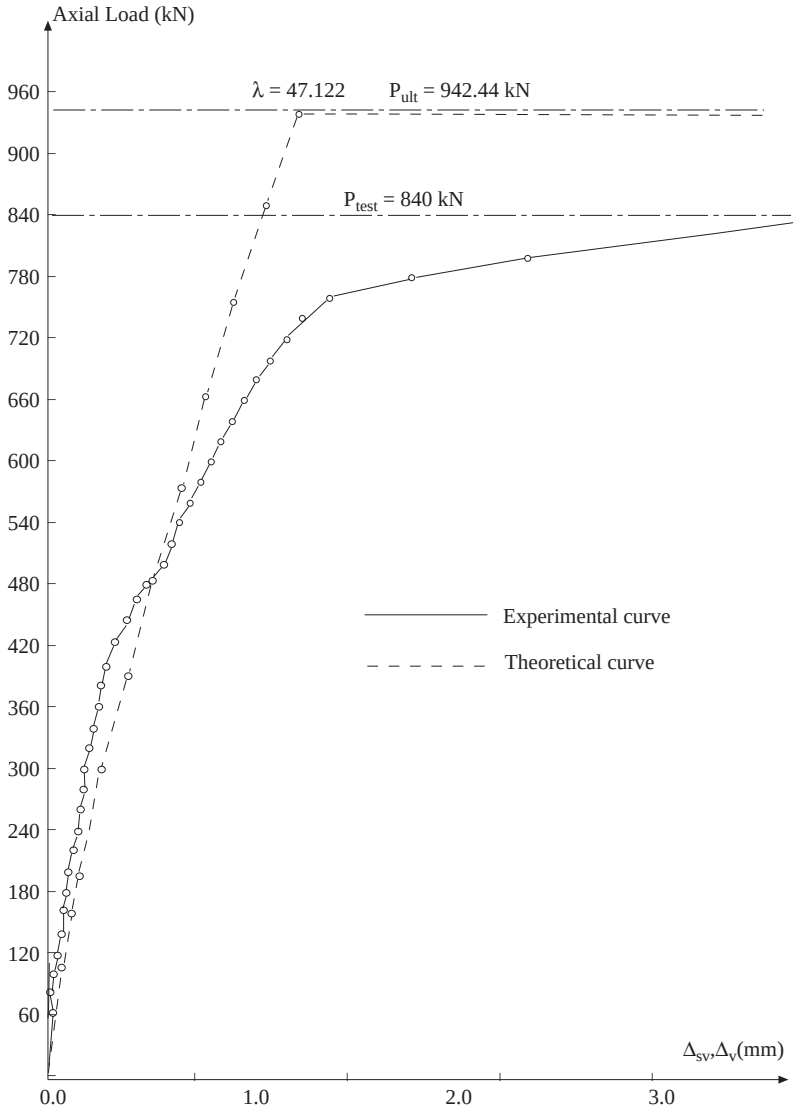

Figure 12. Theoretical and experimental load-vertical displacement curves for test SR2-2

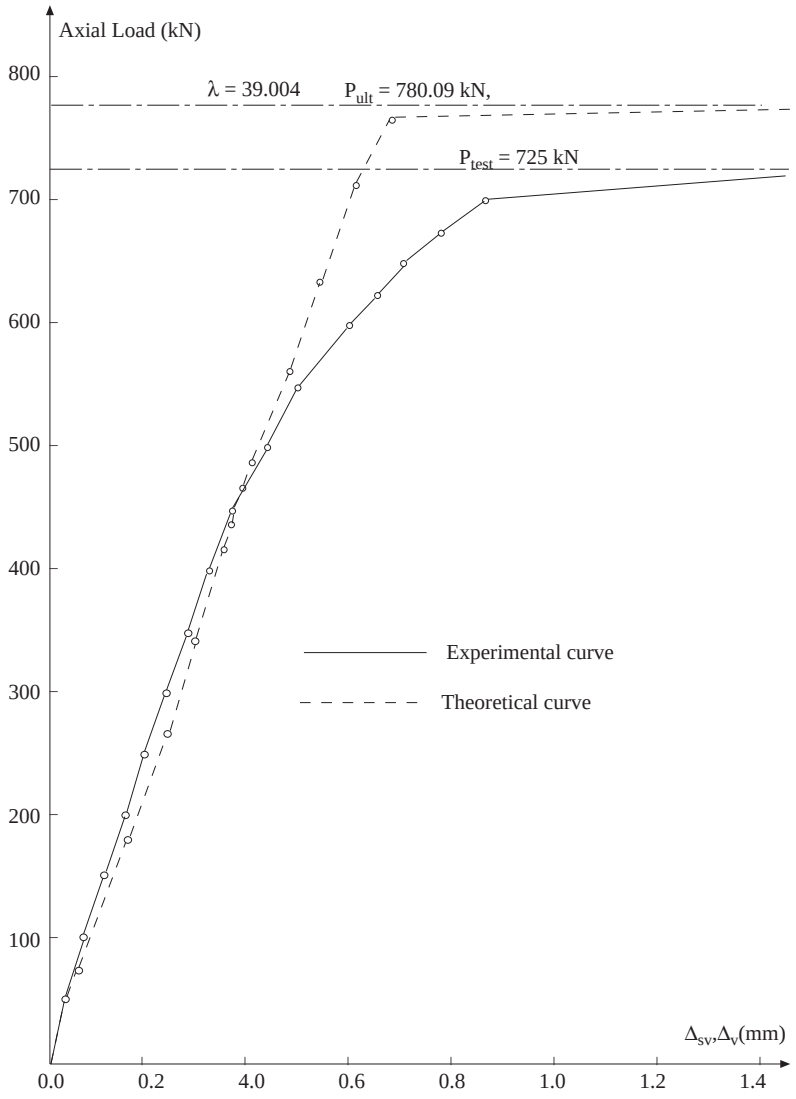

Figure 13. Theoretical and experimental load-vertical displacement curves for test SR7-1

$$P_{ult} = 4\lambda p \tag{54}$$

where λ is the overall load factor, at which all concrete layers yielded due to the ultimate bond stress development on the bar elements along the anchorage length, and p is the working load. It can be seen from Table 1 that the values determined from the theory compare favourably with the experimental results.

By considering the end bearing of the column bars in the base, further theoretical solutions were carried out for a number of tests. These results indicate on average a mere 7% increase at the ultimate load by comparison to the theoretical failure load without end bearing. However, in the solutions the ultimate end bearing resistance was taken as the concrete compressive strength. This is a rough estimate somewhat on the conservative side.

Table 1. Comparison of experimental and theoretical failure loads

Test Specimen No	Concrete Compressive Strength f_{cu}	Experimental Ultimate Load P_{test}	Theoretical Ultimate Load P_{ult}	$\frac{P_{test}}{P_{ult}}$
	N/mm^2	kN	kN	
SR1-1	31.76	365.00	378.50	0.964
SR1-2	32.31	543.70	527.02	1.032
SR1-3	31.13	1400.00	1407.10	0.995
SR2-1	32.96	637.50	695.38	0.917
SR2-2	34.71	840.00	942.44	0.891
SR3-1	34.47	1125.00	1144.41	0.983
SR4-1	30.60	1400.00	1428.68	0.980
SR4-2	31.22	1450.00	1530.71	0.947
SR4-3	29.29	1575.00	1595.94	0.987
SR5-1	29.40	1525.00	1567.68	0.973
SR5-2	32.80	1500.00*	1656.78	0.905
SR6-2	34.70	650.00	708.68	0.917
SR6-3	31.67	680.00	755.86	0.900
SR6-4	32.02	756.20	820.02	0.922
SR7-1	32.56	725.00	780.09	0.929
SR7-2	32.67	837.50	918.97	0.911
SR8-1	25.56	525.00	616.68	0.851
SR8-2	21.90	487.50	573.18	0.881
SR8-3	27.82	575.00	631.38	0.911
SR8-4	36.30	667.50	719.58	0.928
Mean				0.936
Coefficient of variation				4.81

* : indicates no bond failure of column bars in the foundation

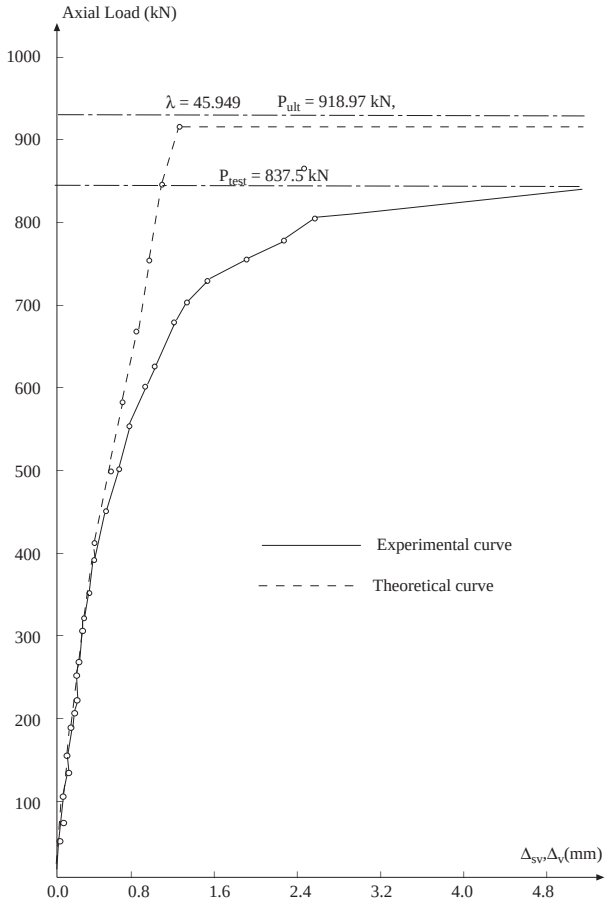

Figure 14. Theoretical and experimental load-vertical displacement curves for test SR7-2

8. Conclusions

On the basis of the theoretical investigation presented in this paper the following conclusions are drawn.

1) The theoretical analysis shows that the maximum and minimum bond stresses are at the top and bottom parts of the anchorage length respectively, and vary nonlinearly in between, which confirms the general trend indicated by the experimental results.

2) The theoretical solutions indicate that the distribution of the bond stress along the anchorage length of the column bars in the base is significantly influenced by the bar stiffness factor K, which is the measure of the compressibility of the bar. As K decreases, i.e. the bar becomes more compressible, the magnitude of the bond stress at the top part of the anchorage length increases, which results in local yield in the concrete at smaller loads and, the proportion of the load transferred to the concrete by bond by the lower part of the bar in the base is significantly decreased. The theoretical analysis also shows that the influence of the K on the distribution of bond stress is more significant for greater anchorage lengths.

3) The proposed method predicts the distribution of the bond stress over the anchorage length of the column bars with reasonable accuracy when compared with the experimental results.

4) The proposed theoretical method determines the vertical displacement of ribbed bars with good degree of accuracy as can be seen by comparison with the experimental results.

5) The failure loads obtained from the theoretical analysis for foundations, are in very good agreement with the test results.

8.1. Notation

a	radius of bar
A_s	cross-sectional area of bar
[C]	compound matrix
[CP]	matrix of coefficients for bar action
[CS]	vertical displacement influence factors matrix for concrete
[DB]	sub-matrix of [CS]
$(\mathrm{DEF})_i$	vertical displacement of concrete at load factor λ^i
E_c	Young's modulus of concrete
E_s	Young's modulus of steel
G_c	shear modulus of concrete
K	bar stiffness factor
M	grid indication number for numerical integration
n	number of cylindrical bar elements
P	axial load on column bar
p	axial working load
P_{test}	experimental ultimate load
P_{ult}	theoretical ultimate load
w_{ij}, w_{ib}	influence factors for vertical displacement at point i due to stresses on element j and bar tip, respectively
w_{bj}, w_{bb}	influence factors for vertical displacement of bartip due to shesses on element j and the bartip, respectively
[Y]	column matrix of constants
[Δc]	vertical displacement matrix of concrete
Δc_b	vertical displacement of concrete under bar tip due to bond stress on bar elements and normal stress on bar tip
Δc_i	vertical displacement of concrete at point i due to bond stress on bar elements and normal stress on bar tip
[Δs]	vertical displacement matrix of bar elements
Δs_v	vertical displacement of column bars
δ	length of bar element
λ	overall load factor
$\lambda_1, \lambda_2, \lambda^i$	load factors
σ	normal stress in column bar
θ	angle
τ	bond stress
τ_b	normal stress on bar tip
τ_u	ultimate bond stress
v_c	Poisson's ratio of concrete
ϕ	nominal bar diameter

References

Astill, A. W. and Al-Sajir, D.K., "Compression bond in Column-to-base joints", The Structural Engineer, Vol. 58B, March 1980.

Astill, A. W. and Turan, M., "Compression anchorage stresses in bases", Bond in Concrete - Proceedings of the International Conference on Bond in Concrete held in Paisley, Scotland, Applied Science Publishers, London 1982.

Cairns, J. and Arthur, P. D., "Strength of lapped splices in reinforced concrete columns", Journal of the American Concrete Institute, Proceedings Vol. 76, February 1979.

Cairns, J., "An analysis of the ultimate strength of lapped joints of compression reinforcement", Magazine of Concrete Research, Vol. 31 March 1979.

Ferguson, P. M. and Thompson, J.N., "Development length of high strength reinforcing bars in bond", Journal of the American Concrete Institute, Proceedings Vol. 59, July 1962.

Ivering, J. W., "Bond of tube in semi-infinite elastic solid", Journal of Strain Analysis, Vol. 15, 1980.

Mattes, N.S. and Poulos, H.G., "Settlement of single compressible pile", Journal of the Soil Mechanics and Foundations Division, Proceedings of the American Society of Civil Engineers, SM1, Vol. 95, January 1969.

Mindlin, R. D., "Force at a point in the interior of a semi-infinite solid", Physics, Vol. 7, May 1936.

Poulos, H. G. and Davis, E. H., "The settlement behaviour of single axially loaded incompressible piles and piers", Geotechnique, Vol. 18, 1968.

Rehm, G., "The basic principles of the bond between steel and concrete", Cement and Concrete Association, Translation No. 134, London 1968.

Roberts, N. P. and HO, R.C., "Behaviour and design of tensile lapped joints in reinforced concrete beams", Civil Engineering and Public Works Review, January 1973.

Tephers, R., "Cracking of concrete cover along anchored deformed reinforcing bars", Magazine of Concrete Research, Vol. 31, March 1979.

Turan, M., "The strength of column-to-foundation joints in reinforced concrete", Thesis submitted to the University of Aston in Birmingham for the degree of PhD. March 1983.